Supporting Information

Ligand-effect-induced Oxygen Reduction Reaction Activity Enhancement for Pt/Zr/Pt(111) Surfaces with Tensile Strain Relieved by Stacking Faults

Daisuke Kudo[1], Soma Kaneko[1], Rikiya Myochi[1], Yoshihiro Chida[1], Naoto Todoroki[1], Tadao Tanabe[2], Toshimasa Wadayama[1]*

[1] Graduate School of Environmental Studies, Tohoku University, Sendai 980-8579, Japan

[2] Graduate School of Engineering, Tohoku University, Sendai 980-8579, Japan

KEYWORDS: oxygen reduction reaction; Pt-shell; tensile strain; Pt-Zr surface alloy; stacking fault; arc-plasma deposition; in-plane XRD, cross-sectional STEM

*; corresponding author

TEL: +81-22-795-7320

Email:n-todoroki@material.tohoku.ac.jp

1. Phase diagram of Pt-Zr alloys

Phase diagram of the Pt-Zr bimetallic system[1] was shown in Figure S1. Intermetallic compounds having non-face-centered-cubic (fcc) crystal structures, such as Pt_3Zr, PtZr, Pt_3Zr_5 appear on the phase diagram, accompanied with solid solution of fcc Pt alloys (solid-solution limit of ca. 20 at%). Figure 2 in the manuscript clearly showed the crystal structure of U_3.2nm in near surface region was fcc. Therefore, the Pt-Zr alloy layers located under the surface Pt(111)-shell lattices are Pt-rich fcc alloys with less than ca. 20 at% of Zr.

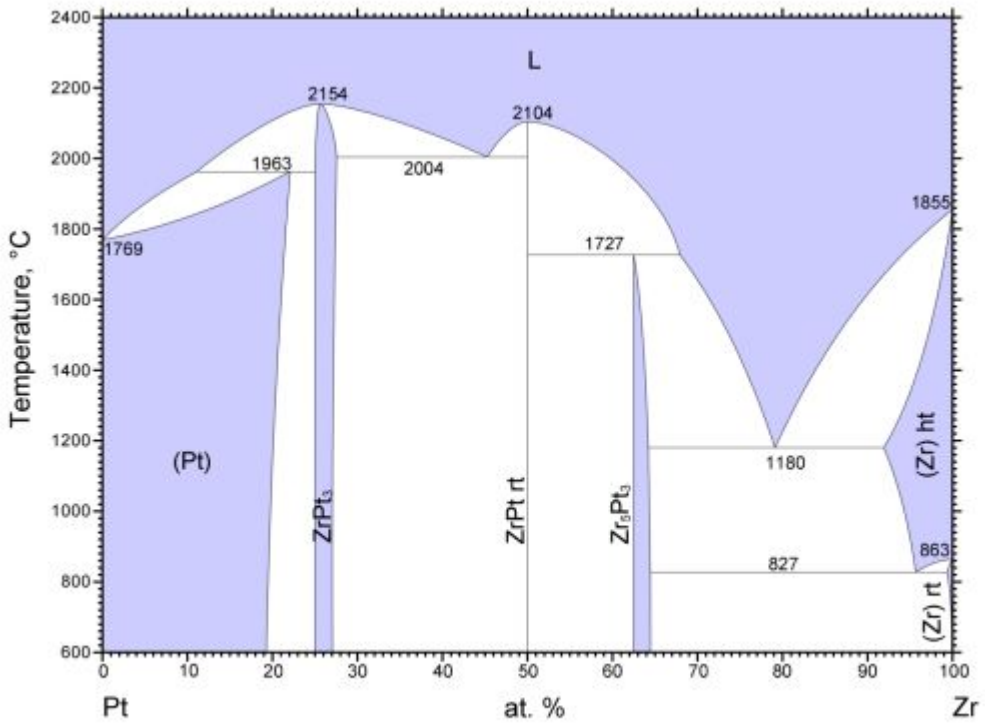

Figure S1. Phase diagram of Pt-Zr bimetallic system.

2. Pt and Zr arc-plasma deposition (APD) sequences

The APD sequences of the Pt/Zr/Pt(111) fabrication are depicted in Figure S2 and described in detail elsewhere.[2] The APD parameters were set to the values in Table S1. The deposition thicknesses of Zr and Pt were monitored by a quartz-crystal microbalance installed in the APD chamber. In this model catalyst deposition sequences, the 1st-layer Zr and 2nd-layer Pt are inserted as "buffer layers" in the nanostructures to mitigate large lattice mismatch between deposited Zr and Pt substrate. If the 3rd Zr-layer directly deposited on the Pt(111) substrate, the Zr lattice would be laterally compressed. Then, in the APD sequences, the buffer layers (1st-layer Zr and 2nd-layer Pt) might work to weaken lattice mismatch of 3rd Zr-layer against underlayer Pt and enable us to epitaxial growth of Pt-shell/Pt-Zr-alloy nanostructures on the Pt(111) substrate.

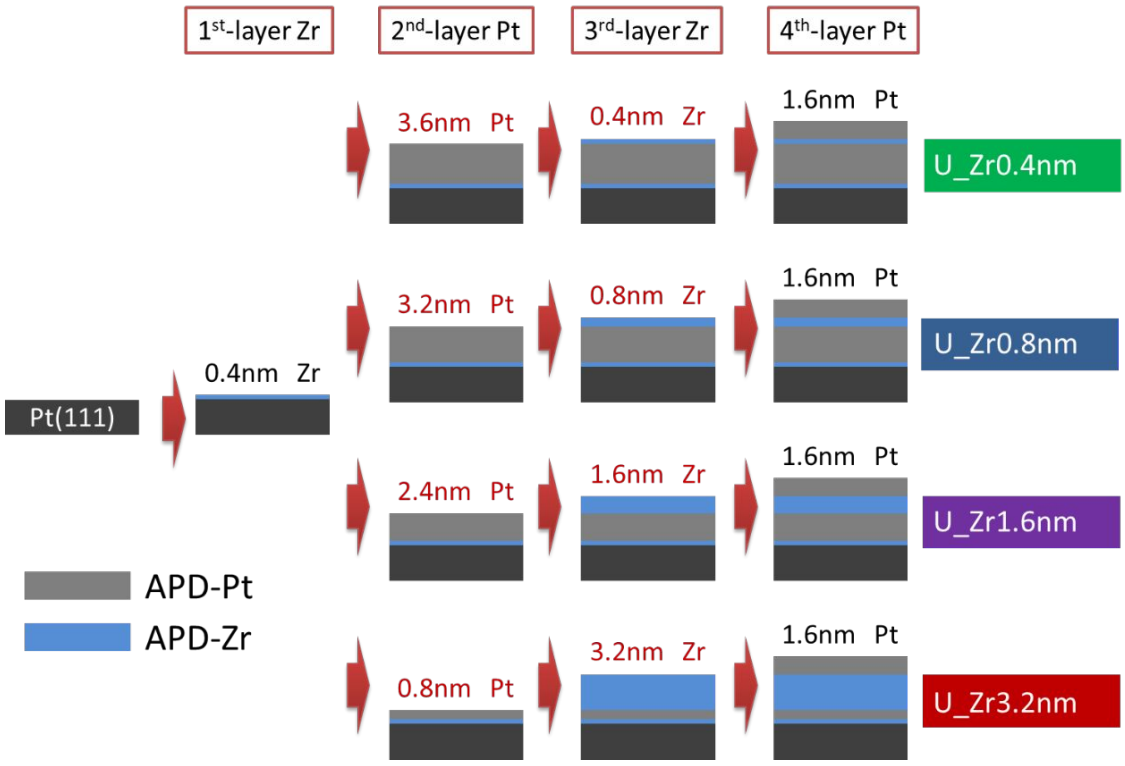

Figure S2. Deposition sequences of Zr and Pt on the clean Pt(111) substrate.

Table S1 APD parameters in the Pt/Zr/Pt(111) surface fabrications.

	Substrate temperature (K)	Arc-voltage (V)	Pulse-frequency (Hz)	Pulse-repetitions for 0.4 nm-thick deposition	Time interval for every 0.4 nm-thick-deposition (s)
Zr	873	70	10	21	60
Pt	873	70	10	25	60

3. In-plane XRD measurements

Figure S3 shows the in-plane layout of the XRD measurements (top), and a zoom-in of the diffraction peaks of Pt(220) on the Pt/Zr/Pt(111) surfaces (bottom). The in-plane XRD measurements were conducted in air and the measurements conditions are detailed elsewhere.[1]

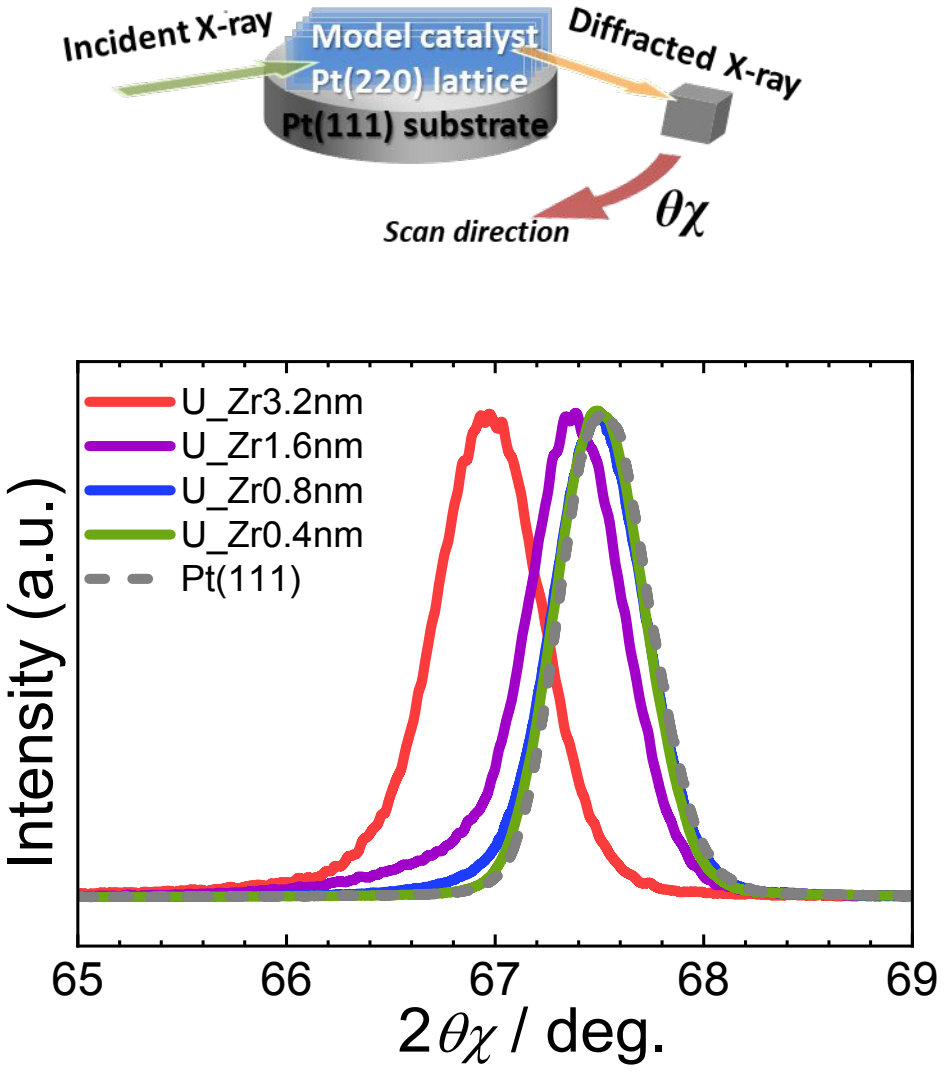

Figure S3. In-plane XRD layout (top) and enlarged XRD pattern of Pt(220) on the Pt/Zr/Pt(111) bimetallic surface (bottom; see Figure 2 of main text) in the interesting range of diffraction angles (35°–69°).

4. Compositional analysis of the near surface region of U_Zr3.2nm

Figure S4 shows STEM-EDS analysis of alloy composition in near surface region of U_Zr3.2nm. The alloy composition of Zr was estimated to be 17 at% in the 2 nm-thick regions (red dashed square) under the Pt(111)-shell. The result suggests that the Zr atoms adjacent to the Pt-shells should be present and, then, contribute to the ORR activity enhancement through the charge transfer between the Pt and Zr atoms (ligand effect).

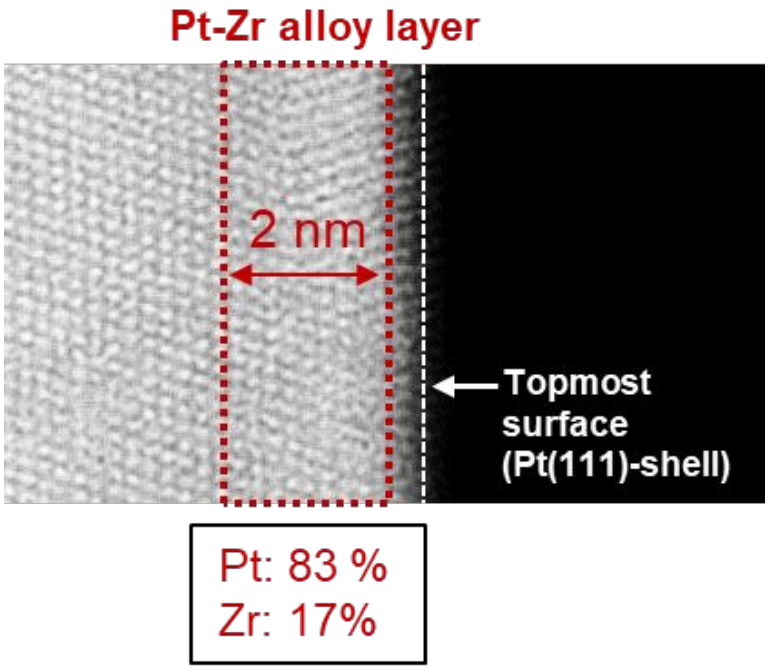

Figure S4. Alloy compositional analysis for U_Zr3.2nm in the 2 nm-thick region (red dashed square) of the Pt-Zr alloy layers under the surface Pt(111)-shell.

5. Anodic current part of the cyclic voltammograms of the Pt/Zr/Pt(111) surfaces in the potential region 0.55–0.9 V.

Figure S5 shows the anodic current parts of the cyclic voltammograms recorded in N_2-purged 0.1 M $HClO_4$ during positive scanning of the surfaces over the potential range 0.55–0.9 V. The peak potentials of the so-called "butterfly" pattern (0.8 V for clean Pt(111)) were relatively insensitive to thickness of the third-layer Zr.

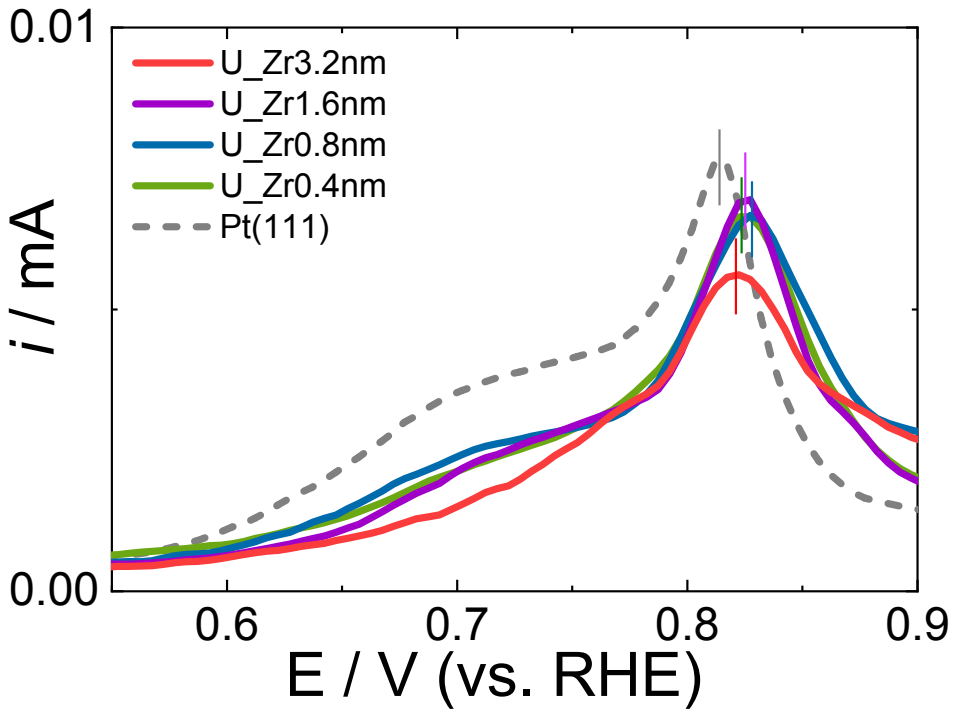

Figure S5. Electrochemical responses of the Pt/Zr/Pt(111) surfaces during positive scanning in the potential range 0.55–0.9 V.

6. LSVs and Tafel plots

The LSV measurements of the Pt/Zr/Pt(111) surfaces under the O_2-saturation of the 0.1M $HClO_4$ solution was conducted after the CV measurements; the results are summarized in Figure S6. The LSV curves collected at 1600 rpm were positively shifted by half-wave potentials, relative to clean Pt(111) (gray dashed line), indicating higher ORR activity than in clean Pt(111). Corresponding Tafel slopes for The Pt/Zr/Pt(111) surfaces are almost same except for U_Zr0.4nm.

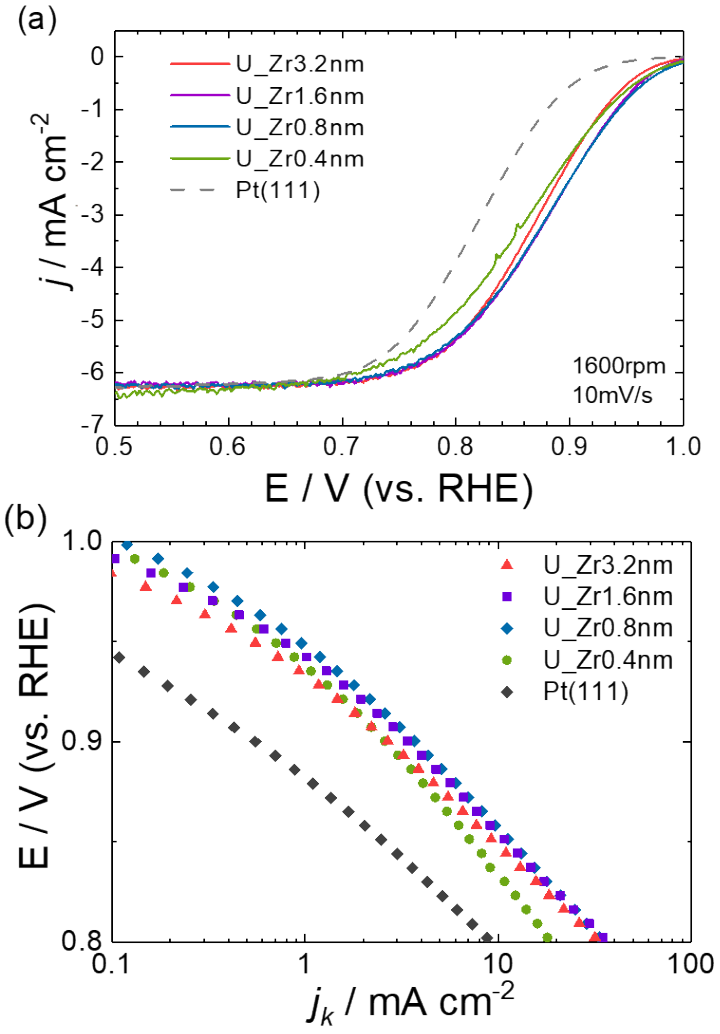

Figure S6. (a) Linear-sweep voltammograms recorded at a disk rotation rate of 1600 rpm in O_2-saturated 0.1 M $HClO_4$ (scan rate = 5 mV/s; positive scan direction). (b) Corresponding Tafel plots.

7. XP spectra of U_Zr3.2nm in the Zr*3d* and Pt*4f* regions before and after 5000 potential cycles

X-ray photoelectron spectroscopic (XPS) analysis of the model Pt(111) shells was performed in another UHV chamber equipped with a semi-spherical electron energy analyzer and an X-ray source (SPECS PHOIBOS100 and XR50). Li et al.[3] reported the surface chemical states of $Pt_3Zr(111)$ and the Zr $3d_{5/2}$ band located at 179.6 eV. As shown in Figure S7, the binding energy of the Zr $3d_{5/2}$ band in pristine U_Zr3.2nm (red) well matches the published binding energy of Zr $3d_{5/2}$ in Pt_3Zr. The Pt$4f_{7/2}$ band of pristine U_Zr3.2nm can be deconvoluted to Pt^0 (red), Pt^{2+} (blue) and the former deconvoluted band shifts ca. 0.15 eV positively, suggesting electronic charge transfers between the Pt and Zr atoms in the surface vicinity. Even after applying the 5000 PCs, both the Pt 4*f* and Zr 3*d* bands remained nearly unchanged. The change in Zr bands by the PCs , suggests that the surface Zr was relatively stable against the PCs through passivation in this condition (the PCs at pH=1).

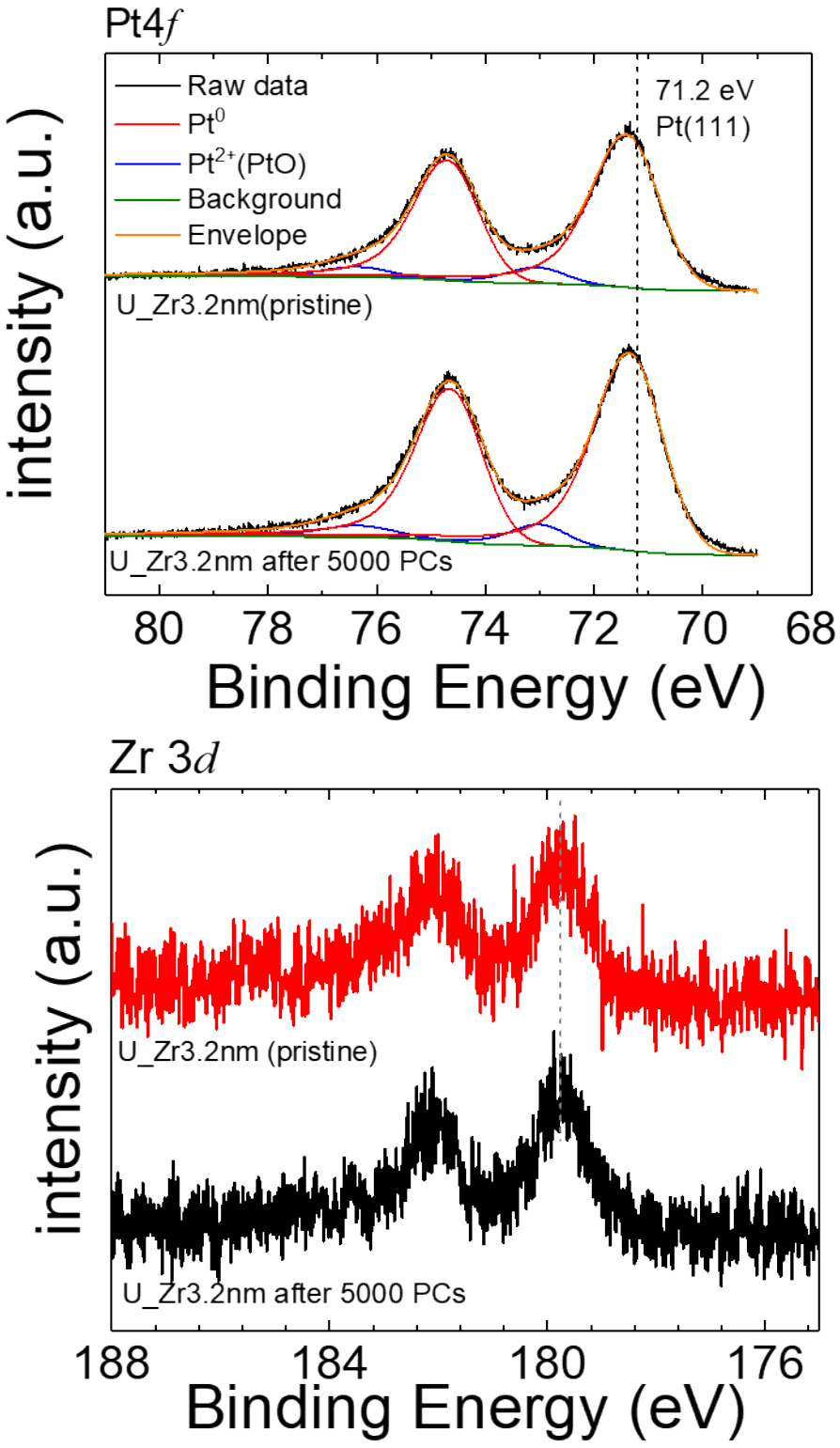

Figure S7. XPS spectra of the Pt*4f* (top) and Zr*3d* (bottom) bands in U_Zr3.2nm before and after 5000 PCs.

References

(1) Xu, Y.; Yamazaki, M.; Villars, P. Inorganic Materials Database for Exploring the Nature of Material. *Japanese Journal of Applied Physics* 2011, 50, 11RH02.

(2) Kaneko, S.; Myochi, R.; Takahashi, S.; Todoroki, N.; Wadayama, T.; Tanabe, T. Ultrahigh Vacuum Synthesis of Strain-Controlled Model Pt(111)-Shell Layers: Surface Strain and Oxygen Reduction Reaction Activity. *J. Phys. Chem. Lett.* 2017, 8, 5360-5365.

(3) Li, H.; Choi, J.-I. J.; Mayr-Schmölzer, W.; Weilach, C.; Rameshan, C.; Mittendorfer, F.; Redinger, J.; Schmid, M.; Rupprechter, G. Growth of an Ultrathin Zirconia Film on Pt3zr Examined by High-Resolution X-Ray Photoelectron Spectroscopy, Temperature-Programmed Desorption, Scanning Tunneling Microscopy, and Density Functional Theory. *J. Phys. Chem. C* 2014, 119, 2462-2470.